21st Australasian Fluid Mechanics Conference
Adelaide, Australia
10-13 December 2018

Boundary layer transition on the surface of a cylinder in oscillatory flow

X. Ju[1], H. An[1], L. Cheng[1, 2] and F. Tong[1]

[1]School of Engineering
The University of Western Australia, Crawley, Western Australia 6009, Australia

[2]DUT-UWA Joint Research Centre
State Key Laboratory of Coastal and Offshore Engineering
Dalian University of Technology, Dalian, Liaoning 116024, China

Abstract

The phenomena of sinusoidally oscillatory flow around a stationary circular cylinder are very rich and are of great importance to both practical engineering and fundamental studies. In this paper, two-dimensional (2D) numerical simulations are conducted for oscillatory flows around a circular cylinder. Drag crisis, which has been previously reported in unidirectional flows, is captured and the transition to turbulence on the cylinder surface is observed. The boundary layer transition is demonstrated by the pressure distribution on cylinder surface, along with the movements of stagnation point and separation point.

Introduction

The transition of plane-wall boundary layer in oscillatory flow has been the subject of many investigations for decades. One way of illustrating the laminar-to-turbulent transition is to display the friction coefficient as function of Reynolds number (in boundary-layer flows, $Re_b = \frac{aU_{0m}}{\nu}$, where U_{0m} is the maximum value of the free-stream velocity, a is the amplitude of the free-stream motion and ν is the kinematic viscosity of the fluid). The bed-shear-stress experiences turbulence first just prior to the bed shear-stress reversal and then spreads towards smaller and smaller values of phase with increasing Re_b. Jensen et al. [4] explained it as the adverse pressure gradient becomes relatively large and the velocity of near-bed fluid particles becomes relatively small at the phase value where bed shear stress reverses, so that a favourable environment forms for the initiation of turbulence. The boundary-layer properties change markedly with respect to Re_b near the bed, and the manner in the turbulence quantities change is exactly the same as in steady boundary-layer flows.

In offshore engineering, circular shaped structures are used widely, such as pipelines, risers and pile foundations etc. Thus comprehensive researches on a circular cylinder in sinusoidal oscillatory flow or waves have been carried out during the past few decades. The two related dimensionless parameters are the Keulegan–Carpenter number (KC) and Strokes number (β), which are defined as

$$KC = \frac{U_m T}{D}, \beta = \frac{Re}{KC} = \frac{D^2}{\nu T} \quad (1,2)$$

where $Re = \frac{U_m D}{\nu}$, U_m is the maximum oscillation velocity, T is the period of the oscillation, and D is the diameter of the cylinder.

Oscillatory flow phenomena around a stationary circular cylinder are rather rich. These include acoustic streaming [7,8,14], Honji instability [2], dipole tubes, quasi-coherent structures, and transition to turbulence [11,12]. It is believed that every possible combination of KC and β is of great importance in both practical and fundamental study and touches certain unique aspects of time-dependent flows [13].

For relatively small KC and β, eight regimes of flow has been identified experimentally by Tatsuno and Bearman [16]. The Honji instability was studied by An [1] and the spacing between Hongji vortices have been investigated. Interestingly, from a physical point of view, Justesen [6] pointed out that as $KC \to 0$, the flow amplitude will become so small with respect to D that the flow will not be able to feel the geometry of the wall below it, whether the wall is a cylinder surface or a flat plate, and the separation phenomenon would lead to simultaneous flow reversal over the entire cylinder surface in this extreme condition.

For relatively large KC (up to 150) and Re (up to 7×10^5), Sarpkaya [9] presents the results of an extensive experimental investigation on smooth and sand-roughened circular cylinders. He concluded that, the drag coefficient undergoes a 'drag crisis' and then rises to a nearly constant value within the range of Re and KC tested, while the inertia coefficient also undergoes an 'inertia crisis' at Re values corresponding to the 'drag crisis' and then asymptotically decreases. Zdravkovich [18] describes the process of the 'drag crisis' in terms of the point of transition to turbulence found in the cylinder wake. The transition to turbulence happens closer to the rear end of the cylinder as Re increases. At Re just below that for the 'drag crisis', two transition points can be observed, which are in the shear layer just beyond the point of separation on each side of the cylinder. These points move as Re further increases, causing one or both separation points to jump from one position to another. This results in a drop in drag, caused by the narrowing of the wake behind the cylinder.

Sarpkaya [10] compared his experimental results with the theoretical predictions of Stokes and Wang, which were in good agreement with the Stokes–Wang analysis for 2D attached and laminar flow conditions. He divided the flow into four broad regimes according to KC. However the regime where drag coefficient decreases was not discussed. Sarpkaya [13] measured the positions of the separation points experimentally by examining a smooth circular cylinder immersed in a sinusoidally oscillating flow for a constant value of β as KC increased from the marginally stable to fully separated region. He pointed out that the separation is three-dimensional, far from being a single eruption of a double sided single shear layer or the departure of dye filaments from the surface of a self-contained bubble.

The existing literature demonstrates that there is also a boundary layer transition related drag crisis for circular cylinder in oscillatory flow. Very little information is available about how the boundary layer transition happens on the cylinder surface. This motivates present work. In this paper, we focus on a smooth cylinder in the oscillatory flow at Re between 10^3 and 10^5 and $KC = 10$. The transition to turbulence is studied numerically. The flow structures on the cylinder surface are discussed in detail to shed light on the boundary layer transition process.

Numerical Method

Governing Equations and the Numerical Model

Large Eddy Simulation model is used in this study. Numerical simulations of oscillatory flow around a circular cylinder have been carried out by solving the filtered incompressible Navier–Stokes (NS) equations using the Open-source Field Operation and Manipulation (OpenFOAM). The NS equations and the continuity equation can be expressed as

$$\frac{\partial \bar{u}_i}{\partial t} + \bar{u}\frac{\partial \bar{u}_i}{\partial x_j} + \frac{1}{\rho}\frac{\partial \bar{p}}{\partial x_i} = \frac{\partial}{\partial x_j}\left([\nu + \nu_t]\frac{\partial \bar{u}_i}{\partial x_j}\right) \quad (3)$$

$$\frac{\partial \bar{u}_i}{\partial x_i} = 0 \quad (4)$$

where the velocity component u_i is decomposed into a filtered velocity ($\bar{u}_i$) and a subgrid-scale velocity (u_i'), $\bar{u}_i = u_i - u_i'$, the same operation applies for pressure, and ν_t is the subgrid-scale turbulent viscosity. A homogeneous dynamic Smagorinsky model was adopted. The finite volume method is used and pressure-velocity coupling is achieved following the Pressure Implicit with Splitting of Operators (PISO) method. The convection terms are discretised using the Gauss cubic scheme, while the Laplacian and pressure terms in the momentum equations are discretised using the Gauss linear scheme. The Euler implicit scheme is adopted for the temporal discretisation [17].

A rectangular computational domain with total size of $40D \times 20D$ and a single cylinder placed in the middle is employed in this study. A close-up view of the 2D mesh near the cylinder is shown in Figure 1(a).

The initial values of flow velocity and pressure are set to zero in the whole domain. Flow velocity and pressure boundary conditions on the left boundary are set to $U_x(t) = U_m \sin\left(\frac{2\pi}{T}t\right)$, $U_y(t) = 0$ and $\frac{\partial p}{\partial x} = U_m \frac{2\pi}{T}\cos\left(\frac{2\pi}{T}t\right)$.

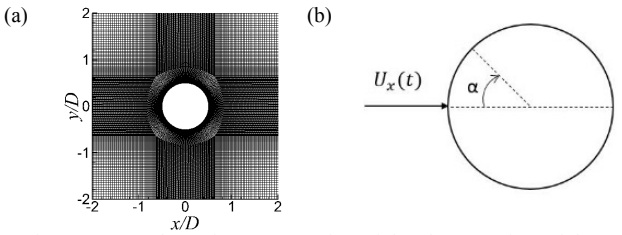

Figure 1. (a) Schematic representation of the close-up view of the 2D mesh near the cylinder. (b) the definition of α, which is the angle on the cylinder surface measured from the upstream stagnation point.

The velocity gradients in the x direction are set to zero and the pressure is specified as a reference value of zero on the right boundary. The symmetry boundary condition is adopted on the two boundaries parallel to the flow direction. And non-slip boundary condition is applied on the cylinder surface.

It is known that the boundary layer transition on the cylinder is a three dimensional flow phenomenon, but it is believed that 2D simulations can reveal the features of boundary layer transition from laminar to turbulent to certain extent as demonstrated by [2] and [15]. Three-dimensional simulations are still required to achieve more accurate understanding about the transition process and this work is being extended to three-dimensional.

Mesh Dependency Check

The mesh dependency check includes the dependency on the mesh resolution in both radial and circumferential directions. Four meshes, as shown in Table 1, with total mesh number ranging from 80,740 to 196,724 have been generated by changing the mesh distribution around the cylinder surface. To make sure the sufficient resolution in the radial direction from the cylinder surface, Δ/D (the first layer mesh from cylinder) was set to keep y+ less than 1. From mesh 2 to mesh 4, Δ/D was kept constant while N_c (the number of cells on the cylinder surface) is refined in order to check that the resolution in the circumferential direction on the cylinder surface is sufficient to capture the transition process on it. A comparison of the simulation results based on the four meshes is given in Table 1. In the table, the total inline force on a body is decomposed into two parts, the drag and inertia components, based on the Morison Equation,

$$F = \frac{1}{2}\rho D C_D |U(t)|U(t) + \rho\frac{\pi D^2}{4}C_M\frac{dU(t)}{dt} \quad (5)$$

where F is the inline force on the cylinder, $U(t)$ is the free stream velocity, C_M is the inertia coefficient and C_D is the drag coefficient. It can be seen that from mesh 2 to mesh 4, C_D and C_M varied by 2.17% and 2.45%, respectively. The root-mean-square of inline force ($C_{In,rms}$) varied less than 2.5% among these four meshes. Reasonable agreement between the meshes demonstrates that a good mesh convergence has been achieved. By taking the efficiency into account, mesh 2 has been selected for the rest of the simulations reported in this work.

Mesh	N_v	N_c	Δ/D	C_D	C_M	$C_{In,rms}$
1	80 740	236	1.48e-4	0.75	1.68	1.320
2	121 924	400	1.13e-4	0.92	1.63	1.325
3	159 324	600	1.13e-4	0.97	1.58	1.327
4	196 724	800	1.13e-4	0.90	1.59	1.293

Table 1. Mesh-independent study on a circular cylinder in oscillatory flow at (Re, KC) = (10^5, 10) on the total element of cells (N_v), the number of cells on the cylinder (N_c), the size of the first layer grid next to the cylinder surface (Δ/D), C_D, C_M, and $C_{In,rms}$.

Results and Discussion

Inertia and Drag Coefficient

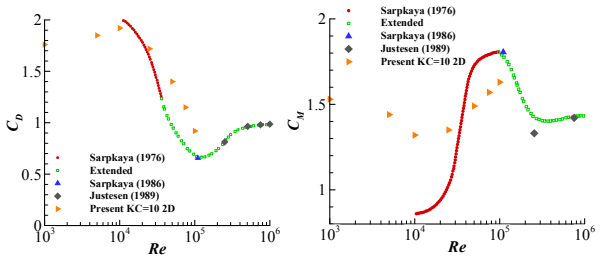

Figure 2. Comparison of C_D and C_M from numerical simulations with experimental data from Sarpkaya [9,10] and Justesen [5] at $KC = 10$.

Numerical simulations have been conducted at Re up to 10^5 for $KC = 10$ in order to capture the transition to turbulence on the surface of a circular cylinder. The force coefficients given by Sarpkaya [9,10] and Justesen [5] are plotted in Figure 2 together with the present numerical results. From Figure 2, a gradually increasing trend can be captured from $Re = 10^3$ to 10^4 for C_D in the present results. Both numerical and experimental results suggest that C_D decreases when Re approximately increases from 10^4 to 10^5, which corresponds to the 'drag crisis'. After that, the experimental data indicates C_D rises and reaches a plateau when Re is about 4×10^5. On the other hand, C_M decreases with increasing Re from 10^3 to 10^4 and then starts to increase at the same value of Re when C_D drops. The experimental data shows a slightly rise after $Re = 2\times10^5$. The numerical results appear to be in fair agreement with the experiment data.

Flow Features

Figure 3 shows the vortex shedding process in one oscillation period for $KC = 10$. In the following, the ambient flow is in

the horizontal direction. In the interval of $[nT \sim +\frac{2}{4}T]$, the flow travels from left to right, whereas it is from right to left in the interval $[+\frac{2}{4}T \sim +\frac{4}{4}T]$.

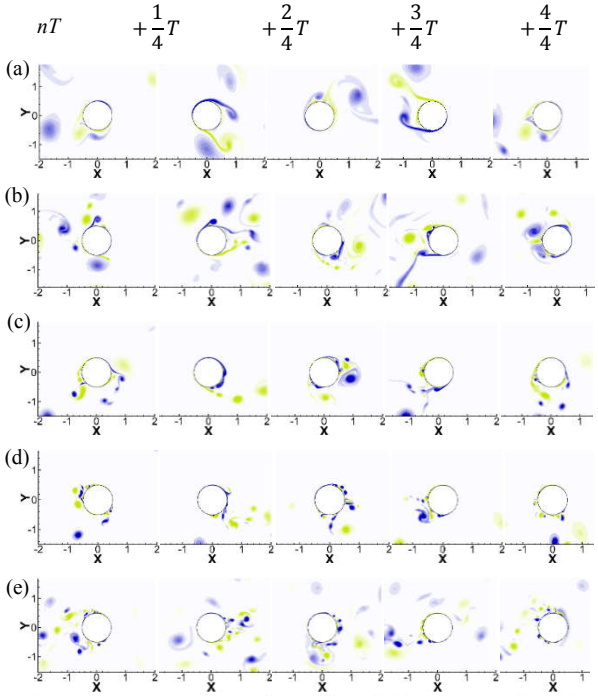

Figure 3. Instantaneous oscillatory flow field around a cylinder in one oscillation period for KC = 10, visualized using vorticity contours at levels between -20 (blue colours) and 20 (green colours), at different Re: (a) Re = 10^3; (b) Re = 5×10^3; (c) Re = 10^4; (d) Re = 5×10^4; (e) Re = 10^5.

From Figure 3(a) at Re = 10^3, it is noticeable that the shear layer on the cylinder surface is quite smooth. At Re = 5×10^3, as shown in Figure 3(b), small vortices appear at the far end of each shear layer. With further increases in Re, the shear layers become more unstable and small vortices appear on the surface of the cylinder (Figure 3(c) and (d)), which indicates a transition from laminar to turbulent in the shear layer. This transition leads to a delay of the separation of flow from the cylinder surface casing a substantial reduction in the drag force (as shown in Figure 2). When Re reaches 10^5, the flow field become increasingly turbulent (Figure 3(e)).

Pressure Distribution and KH Vortices

In order to capture the velocity and pressure distribution on the cylinder surface, 120 probes have been placed around the cylinder. As shown in Figure 4, pressure distribution around the cylinder in two oscillation periods for KC = 10, Re = 10^5 is displayed by using pressure contours at levels between -12 (blue colour) and 12 (red colour). C_P is pressure coefficient around the cylinder surface which is defined as

$$C_P = \frac{p-p_\infty}{p_0-p_\infty} \qquad (6)$$

where p_∞ is the pressure in the freestream and p_0 is the stagnation pressure. C_P' is the pressure difference between C_P and the background sinusoidal pressure. It is understood that the pressure changes are corresponding to the shedding of vortices. Therefore, the small peaks in the pressure signal indicate the small scale vortices shed from the surface of the cylinder. After taking away the background sinusoidal pressure, as shown in Figure 4, the high frequency pressure perturbation can be easily captured. From Figure 4(b), at α = 315°, a dozen of peaks can be noticed in the plot with $\varphi \in$ [5/8, 7/8] (φ is the phase angle of the oscillation). In order to find out in which phase angle of the oscillation and what position on the cylinder that transition happens, we have counted the peaks in C_P' signal of each probe within a relative long time (i.e. 100 oscillation periods) and plotted in Figure 5.

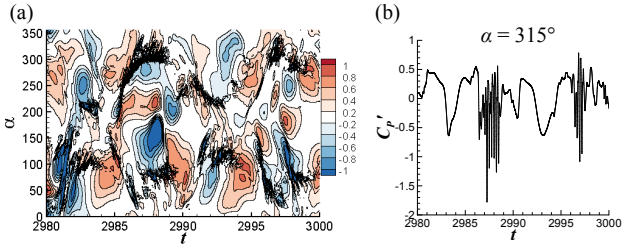

Figure 4. Pressure distribution after data processing of an oscillating cylinder in 2D simulations in two oscillation periods at (Re, KC) = (10^5, 10): (a) pressure C_P' visualised using contours; (b) pressure time history measured at α = 315°. C_P' is the pressure difference between C_P and the background sinusoidal pressure.

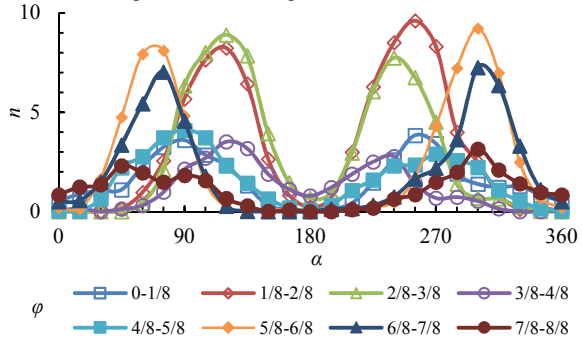

Figure 5. Number of small peaks in the pressure signal per oscillation cycle at (Re, KC) = (10^5, 10). α is the angle on the cylinder surface and φ is the phase angle of the oscillation, sampled in 100 periods.

As shown in Figure 5, for $\varphi \in$ [0, 1/8], the ambient flow starts to accelerate from left to right and the transition happens at a position of roughly 90° and 255°. For $\varphi \in$ [1/8, 2/8], the ambient flow continues accelerate and reaches the maximum velocity. It is noticeable that the number of small peaks for $\varphi \in$ [1/8, 2/8] is more than twice of that for $\varphi \in$ [0, 1/8]. The transition happens at a position around 120° and 255°. When the ambient flow begins to decelerate, the transition point moves to 120° and 240°. And more peaks are found at the position of 120° than 240° for $\varphi \in$ [2/8, 3/8]. For $\varphi \in$ [3/8, 4/8], the ambient flow continues decelerate and the flow velocity reaches zero. The transition happens at the same position of that for $\varphi \in$ [2/8, 3/8]. However, the number of peaks drops to a similar level of that when $\varphi \in$ [0, 1/8], which is less than half of the number for $\varphi \in$ [2/8, 3/8]. For $\varphi \in$ [4/8, 8/8], the ambient flow reverses and starts to travel from right to left. The transition points of the cylinder moves from 90° and 270° for $\varphi \in$ [4/8, 5/8], to 75° and 300° for $\varphi \in$ [5/8, 7/8], and then to 45° and 300° for $\varphi \in$ [7/8, 8/8]. This demonstrates that transition mostly occurs during the acceleration stage just before the velocity decelerates, where there are significant more peaks in the pressure signal.

Pressure Perturbation and Separation point

Another interesting phenomenon in Figure 4(a) is that between α = 220° and 340° in the half oscillation period t = 2985~2990, the perturbation in the pressure signal on the bottom of the cylinder has an obvious trend of traveling to the large value of α. The initial angle of the perturbation rises from approximately t = 2986.6 to 2987 as the ambient flow velocity increases. It reaches the maximum value just after the velocity comes to its maximum value, and then stays in the similar range until about t = 2988.6. Figure 6 has amplified the bottom of the cylinder for t = 2985.6 ~ 2988.6 when the perturbation in the pressure signal has been observed. For clarification, the range of perturbation has been labelled in

each figure. From Figure 6, we can conclude that the perturbation in the pressure signal is mainly caused by the small scale vortices very close to the cylinder. Here, we have plotted the lines where the shear stress equals to 0 in Figure 7 in half period. The zero shear stress lines agree well with the figure of pressure distribution. This confirmed that the traveling of the perturbation in the pressure signal is mainly due to the traveling of the separation point.

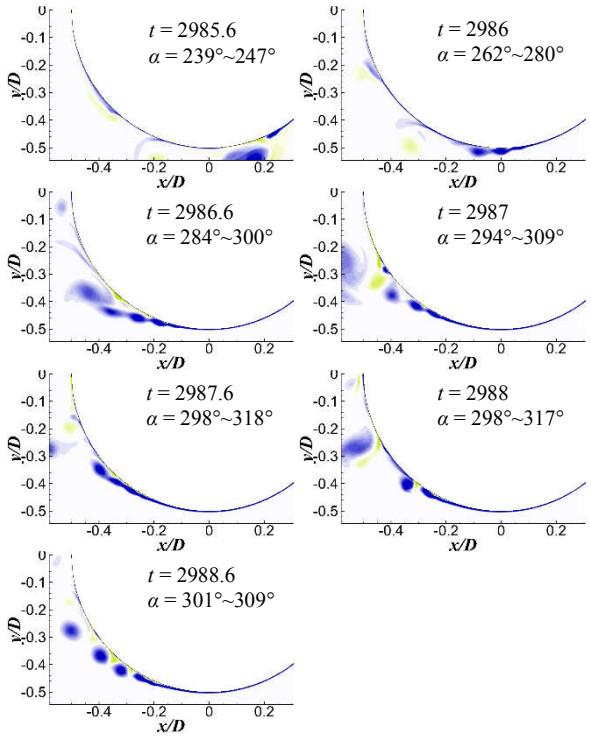

Figure 6. Zoom in for instantaneous flow field between t = 2985.6 ~ 2988.6 at (Re, KC) = (10^5, 10). Time and the range of perturbation in the pressure signal has been labelled in each figure.

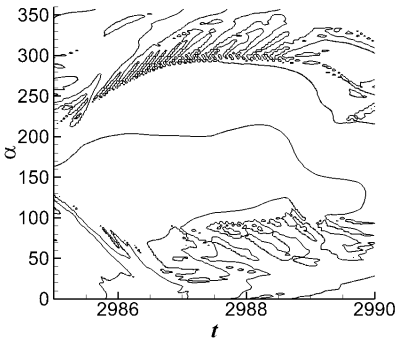

Figure 7 The lines of zero shear stress on the cylinder in half period at (Re, KC) = (10^5, 10).

Conclusions

Two-dimensional numerical simulations are conducted on a cylinder in oscillatory flow at Re = 10^3 ~ 10^5 and KC = 10. The numerical results are in fair agreement with the experiment data. Drag crisis is captured. The transition to turbulence is observed in the flow field and quantified by analysing pressure perturbations around the cylinder. The transition points in terms of phase angle in the oscillation period and position on the cylinder surface are studied. Moreover, the traveling of the perturbation in the pressure signal is shown mainly due to the traveling of the separation point.

Acknowledgments

The first author would like to acknowledge the support from the Australian Government and the University of Western Australia by providing IPRS and APA scholarships for a doctoral degree, as well as the Australia–China Natural Gas Technology Postgraduate Research Scholarships from the Australian and Western Australian Governments, the North West Shelf Joint Venture Partners and the Western Australian Energy Research Alliance. The second authors would like to acknowledge the support from the Australian Research Council through Discovery Early Career Research Award (DE150100428). Computational resources were provided by the Pawsey Supercomputing Centre with funding from the Australian Government and the Government of Western Australia.

References

[1] An, H., Cheng, L. & Zhao, M., Direct numerical simulation of oscillatory flow around a circular cylinder at low Keulegan–Carpenter number, *J. Fluid Mech.*, **666**, 2011, 77–103.

[2] Chopra, G., & Mittal, S., The intermittent nature of the laminar separation bubble on a cylinder in uniform flow, *Computers & Fluids*. **142**, 2017, 118–127.

[3] Honji, H., Streaked flow around on oscillating circular cylinder. *J. Fluid Mech.*, **107**, 1981, 507–520.

[4] Jensen, B. L., Sumer, B. M., & Fredsøe, J., Turbulent oscillatory boundary layers at high Reynolds numbers, *J. Fluid Mech.*, **206**, 1989, 265–297.

[5] Justesen, P., Hydrodynamic forces on large cylinders in oscillatory flow, *Journal of waterway, port, coastal, and ocean engineering*, **115**(4), 1989, 497–514.

[6] Justesen, P., A numerical study of oscillating flow around a circular cylinder, *J. Fluid Mech.*, **222**, 1991, 157–196.

[7] Lighthill, M. J, Acoustic streaming. *J. Sound Vib.*, **61**, 1978, 391–418.

[8] Riley, N., The steady streaming induced by a vibrating cylinder. *J. Fluid Mech*. **68**, 1975, 801–812.

[9] Sarpkaya, T., January. In-Line & Transverse Forces, On Cylinders In Oscillatory Flow At High Reynolds Numbers, *Offshore Technology Conference*, 1976.

[10] Sarpkaya, T., Force on a circular cylinder in viscous oscillatory flow at low Keulegan–Carpenter numbers. *J. Fluid Mech*., **165**, 1986, 61–71.

[11] Sarpkaya, T., Coherent structures in oscillatory boundary layers, *J. Fluid Mech.* **253**, 1993, 105–140.

[12] Sarpkaya, T., Experiments on the stability of sinusoidal flow over a circular cylinder, *J. Fluid Mech.*, **457**, 2002, 157–180.

[13] Sarpkaya, T., Structures of separation on a circular cylinder in periodic flow. *J. Fluid Mech.*, **567**, 2006, 281–297.

[14] Schlichting, H., Berechnung ebener periodischer Grenzschichtstromungen. *Phys. Z.*, *33*, 1932, 327–335.

[15] Singh, S. P. & Mittal, S., Flow past a cylinder: shear layer instability and drag crisis, *International journal for numerical methods in fluids*, **47**(1), 2005, 75–98.

[16] Tatsuno, M. & Bearman, P.W., A visual study of the flow around an oscillating circular cylinder at low Keulegan–Carpenter numbers and low Stokes numbers. *J. Fluid Mech.*, **211**, 1990, 157–182.

[17] Tong, F., Cheng, L., An, H. & Griffiths, T., The hydrodynamic forces on a circular cylinder in proximity to a wall with intermittent contact in steady current, *Ocean Engineering*, **146**, 2017, 424–433.

[18] Zdravkovich, M. M., *Flow Around Circular Cylinders*, *vol. 1: Fundamentals* Oxford University Press, 1997.